Journal of
Materials in Life Sciences

Vol. 4 No. 2 (2025)

Full Paper

Synthesis of Niobium-Doped Silica-Titania Composites via Solid-State Method for Photocatalytic Degradation of Methylene Blue

Chui Min Ling[a], Balqisnurain Mohd Zaidi[a], Shin Er Bon[b], Siew Ling Lee[a,c*]

[a] Department of Chemistry, Faculty of Science, Universiti Teknologi Malaysia, 81310 UTM Johor Bahru, Johor, Malaysia.
[b] Department of Physics, Faculty of Science, Universiti Teknologi Malaysia, 81310 UTM Johor Bahru, Johor, Malaysia.
[c] Centre for Sustainable Nanomaterials, Universiti Teknologi Malaysia, 81310 UTM Johor Bahru, Johor, Malaysia.

Article history
Received
25 September 2025
Revised
6 November 2025
Accepted
6 November 2025
Published online
30 November 2025

*Corresponding author
lsling@utm.my

Abstract

The discharge of dye-laden wastewater, particularly from textile industries, poses significant environmental and health hazards due to the persistence of synthetic dyes. This study reports the synthesis, characterization, and photocatalytic evaluation of niobium-doped silica–titania (Nb–SiO_2/TiO_2) composites as efficient photocatalysts for methylene blue degradation under visible light. The composites were synthesized via a combination of sol–gel and solid-state methods with varying niobium concentrations (1–9 mol%). X-ray diffraction (XRD) analysis revealed that pure TiO_2 exhibited a crystalline anatase phase, while Nb–SiO_2/TiO_2 showed amorphous features due to lattice distortion and silica incorporation. UV–Vis diffuse reflectance spectroscopy (DRS) indicated a bandgap widening from 3.05 eV (TiO_2) to 3.58 eV (9% Nb–SiO_2/TiO_2). BET surface area analysis demonstrated a remarkable increase from 4 to 322 m^2/g for the composite, confirming enhanced porosity and reduced agglomeration. Photocatalytic testing showed that 9% Nb–SiO_2/TiO_2 achieved the highest MB degradation efficiency of 65% at 15 ppm and 84% at 5 ppm within 360 minutes. The superior performance is attributed to improved surface area, charge separation, and the synergistic effects of Nb doping and SiO_2 support, suggesting the composite's substantial potential for sustainable wastewater remediation applications.

Keywords: Silica; Titania; Niobium; Methylene Blue; Photocatalyst

1.0 INTRODUCTION

The discharge of wastewater from textile industries has become a major source of environmental contamination and is now a growing global concern [1]. Among various pollutants, methylene blue (MB) is one of the most extensively used synthetic dyes

in the textile, paper, and pulp industries [2]. MB is non-biodegradable and highly persistent in aquatic environments, posing serious ecological hazards to marine organisms and potential carcinogenic risks to humans [1].

Titanium dioxide (TiO_2) is a widely studied semiconductor photocatalyst that has been demonstrated as a viable method for degrading emerging organic contaminants in sewage and industrial effluents [3]. However, its wide bandgap (~3.2 eV) limits its photocatalytic efficiency under visible light irradiation [4, 5]. To address this limitation, various modifications of TiO_2 have been extensively explored, with metal oxide doping emerging as a simple yet effective approach to enhance visible light activity. Niobium oxide (Nb_2O_5) is particularly attractive due to the close similarity of the ionic radii of Nb^{5+} (0.64 Å) and Ti^{4+} (0.61 Å), which allows Nb to substitute Ti in the TiO_2 lattice [6]. Several studies have demonstrated that Nb doping improves charge separation, tailors the bandgap, and enhances the photocatalytic performance of TiO_2 under visible light [6, 7].

In addition to doping, the incorporation of silica (SiO_2) as a support material has been shown to further enhance the photocatalytic properties of TiO_2-based composites. SiO_2 improves surface area, charge separation, and structural stability, while also preventing agglomeration of TiO_2 nanoparticles, thus providing more accessible active sites for photocatalytic reactions [8]. Recent studies have reported that SiO_2–TiO_2 composites achieve higher photocatalytic efficiency than bare TiO_2, particularly due to their larger surface area and better stability [9, 10].

For the synthesis of such composites, sol–gel and solid-state methods are commonly employed because of their simplicity, effectiveness, and ability to produce residue-free materials [11, 12]. However, despite extensive studies on TiO_2 modification, most works have focused either on niobium doping or on SiO_2/TiO_2 composites individually. Minimal research has investigated the synergistic effect of simultaneously doping TiO_2 with niobium while incorporating SiO_2 as a stabilizing support. Investigating this dual modification strategy may provide new insights into tailoring the electronic structure and surface properties of TiO_2, thereby achieving significant improvements in photocatalytic activity under visible light irradiation.

In this study, niobium-doped SiO_2/TiO_2 composites were prepared using a combination of sol–gel and solid-state methods. The structural, optical, and surface properties of the resulting composites were characterized, and their photocatalytic performance was systematically evaluated for the degradation of MB under visible light irradiation.

2.0 EXPERIMENTAL

2.1 Preparation of materials

The sol-gel method was used to synthesize the photocatalysts in this study, which was subsequently followed by the solid-state method and calcination according to the previous research [13, 14]. The primary objective of this investigation was to synthesize the Nb-SiO_2/TiO_2 composites. Moreover, SiO_2/TiO_2 composites without supporting materials and pure TiO_2 were synthesized for comparison analysis to determine the structure of the obtained compounds.

The sol-gel method was employed to synthesize the TiO_2 photocatalyst [13]. The precursor used was titanium isopropoxide (TTIP), which was combined with absolute ethanol as the solvent and acetylacetone as the chelating agent. A clear, light yellowish solution was produced by preparing the mixture in the molar ratio of 1 mol TTIP: 0.5 acac:100 ethanol. The mixture was stirred at 500 rpm at ambient temperature for 2 hours, subjected to evaporation at 80°C, and permitted to be desiccated overnight at 110°C. The desiccated sample was calcined at 500°C for 5 hours to yield TiO_2.

To synthesize SiO_2/TiO_2 composites, the sol-gel technique was used. Solution A was formed by mixing tetraethyl orthosilicate (TEOS), ethanol, HNO_3, and deionized water in a 1:1:0.6:4 molar ratio in a beaker. Solution A was stirred for 30 minutes at room temperature. After that, solution B was prepared with a molar ratio of 0.5 acetylacetone: 1 TTIP: 100 ethanol. An extra 30 minutes were spent stirring solution B. After adding solution B dropwise to solution A, stir for 1 hour. After mixing, the solution was evaporated at 80°C. To prepare SiO_2/TiO_2 composites, the gel was calcined at 500°C for 5 hours following overnight drying at 110°C to eliminate solvents.

Niobium-doped silica/titania composites were synthesized via the solid-state method. The niobium precursor used in the reaction was ammonium niobate(V) oxalate hydrate. The SiO_2/TiO_2 composites with different concentrations (1, 3, 5, 7, and 9 mol%) of niobium precursors were pulverized in a mortar. Niobium-doped silica titania composites were synthesized by calcining the mixture in a muffle furnace at 600°C for 3 hours.

2.2 Characterization of materials

A number of various analysis techniques were applied to evaluate and offer a deeper understanding of the chemical and physical properties of the photocatalysts. The synthesized samples were characterized by using X-ray Diffraction (XRD) analysis utilizing a Bruker Advance D8 X-ray diffractometer with Cu Ka radiation (λ = 1.5406 Å) for the structural identification of the materials. For the optical properties of the photocatalysts, the diffuse reflectance Ultraviolet-Visible spectroscopy with the brand of Shimadzu UV3600 was employed in the presence of barium sulphate as reference materials. The bandgap energy, E_g, was calculated using the Tauc equation and the Kubelka-Munk function, and a graph of $[FR_xhv]^2$ against energy, eV. Thermo Fischer Scientific Sorptomatic 1990 was applied to conduct the surface area and pore size analysis on the synthesized materials. The functional group of the synthesized samples was determined by utilizing Fourier Transform Infrared (FTIR) Spectroscopy through Thermo Scientific Nicolet iS50 spectrophotometer with the assistance of potassium bromide (KBr).

2.3 Photocatalytic Testing

The photocatalytic efficacy of a catalyst was evaluated by degrading the MB solution (15 ppm) under visible light. The experiment sought to assess the impact of contact duration on the rate of MB removal. A 0.10 g catalyst was introduced to 100 mL of MB solution, and the mixture was agitated in the absence of light for 1 hour to attain adsorption equilibrium. The solution was subsequently illuminated by a fluorescent lamp (400-700 nm, peak at 550 nm) for 6 hours. Samples were collected hourly, and the MB concentration was quantified using a UV-Vis spectrophotometer at 664.5 nm. The removal efficiency (R) was determined using the formula in Equation 1:

$$R = \frac{C_{o-}C_{(t)}}{C_0} x\ 100\% \quad (1)$$

Where C_0 denotes the initial concentration (in ppm) and $C_{(t)}$ represents the concentration at time t (in ppm). To identify the optimal catalysis reaction parameter, additional experiments were performed at varying MB concentrations (5-25 ppm) to assess the samples' efficacy under diverse dye loads.

3.0 RESULTS AND DISCUSSION

3.1 X-Ray Diffraction (XRD) Analysis

XRD was employed to examine the crystalline structure of materials, including pure TiO_2 and doped TiO_2 composites. The existing research examines the structural characteristics of pure TiO_2 and Nb-SiO_2/TiO_2, elucidating the impact of doping on crystallinity and morphology. The molar percentage of Nb (1, 3, 5, 7, and 9 mol%) was varied to produce a range of Nb-SiO_2/TiO_2 samples. Simultaneously, pure TiO_2 and 9% Nb-SiO_2/TiO_2 were synthesized for comparative purposes. The XRD patterns of pure TiO_2 and 9% Nb-SiO_2/TiO_2 are illustrated in Figure 1. Pure TiO_2 was produced using the sol-gel technique, and the primary observation was the predominance of the anatase phase at moderate annealing temperatures, characterized by high crystallinity and purity. The peak positions at 2θ = 25.37°, 37.93°, 48.12°, 53.97°, 55.09°, 62.79°, and 75.21° correspond, respectively, to the diffraction planes (101), (004), (200), (105), (211), (204), and (215) of the anatase phase of TiO_2 [15]. The minor peaks near 70° correspond to the (116) and (220) crystallographic orientations of the anatase phase of TiO_2 [16]. The observed diffraction pattern is designated in accordance with the standard XRD pattern of JCPDS No. 21-1272 [17]. Conversely, the 9% Nb-SiO_2/TiO_2 composite sample exhibited a large diffraction hump between 2θ = 15° and 35°, without sharp peaks, indicating an amorphous or weak crystalline structure.

The samples' amorphous characteristics may also result from the minimal quantities of both TiO_2 and Nb present [13]. The broad hump is observed at 2θ = 22° for silica nanoparticles. The lack of distinct peaks confirms the absence of an ordered crystalline structure in the produced silica nanostructures and aligns well with the standard XRD patterns of synthesized SiO_2 nanoparticles [18]. Nb^{5+} doping was recognized to cause lattice distortion and impede crystallite formation in TiO_2, while the inclusion of silica enhances amorphization by offering a scattered matrix and diminishing TiO_2 domain contacts [19]. The decrease in crystallinity may enhance photocatalytic applications, as amorphous materials often provide greater surface area and increased active sites for redox processes.

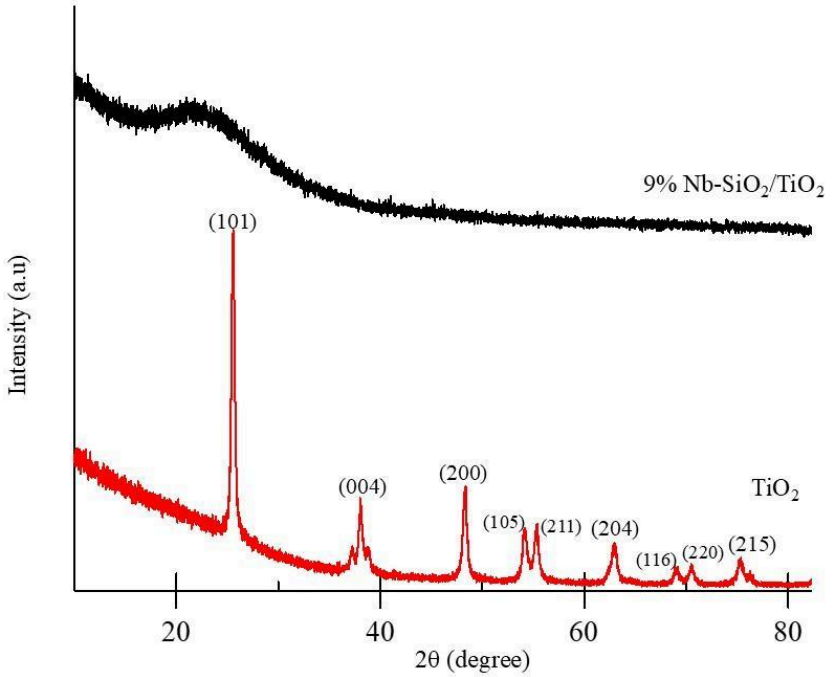

Figure 1 X-ray diffraction patterns of pure TiO_2 and 9% Nb-SiO_2/TiO_2

3.2 UV-Vis Diffuse Reflectance Spectroscopy (UV-Vis DRS)

The optical characteristics of 9% Nb-SiO_2/TiO_2 and pure TiO_2 samples were examined using UV-Vis Diffuse Reflectance Spectroscopy. Figure 2(a) illustrates that pure TiO_2 displayed a broad absorption band between 270 and 400 nm. The hydrated tetrahedral Ti species is represented by the band [6]. On the other hand, the 9% Nb-SiO_2/TiO_2 composite showed less absorption than pure TiO_2.

Figure 2(b) illustrates the graph of $[FR_xhv]^2$ curves as a function of eV, while Table 1 documents the bandgap energy values, E_g, of the samples. The 9% Nb-SiO_2/TiO_2 exhibited a higher E_g of 3.58 eV in contrast to the pure TiO_2, which had an Eg of 3.05 eV. The bandgap of pure TiO_2 is lower than that of pure anatase TiO_2 (3.20 eV), which approaches the typical bandgap of the rutile phase. This redshift in the absorption edge indicates that Nb^{5+} doping and the SiO_2 support significantly modified the electronic structure of TiO_2. The 9% Nb-SiO_2/TiO_2 sample indicates an optical bandgap increase by clearly shifting the absorption edge to higher energy (blue shift). The detected blue shift in the Nb-SiO_2/TiO_2 composite is probably attributable to the Burstein-Moss phenomenon. This phenomenon "fills" the lower conduction band states, necessitating higher energy photons to excite electrons from the valence band, hence enlarging the apparent bandgap [9]. Nb^{5+} ions function as electron donors when integrated into the TiO_2 lattice, hence augmenting the carrier concentration in the conduction band. The addition of Nb^{5+} and SiO_2 may inhibit mid-gap defect states, leading to a more refined electronic transition and a more distinct absorption edge. The incorporation of SiO_2 is recognized to enhance the surface area and optimize the dispersion of TiO_2 nanoparticles, thus affecting the optical characteristics by minimizing aggregation and preserving the anatase phase [10]. In addition, SiO_2 may assist in stabilizing the TiO_2 lattice and inhibiting the production of rutile, thus preserving the anatase phase, which is more effective for photocatalysis.

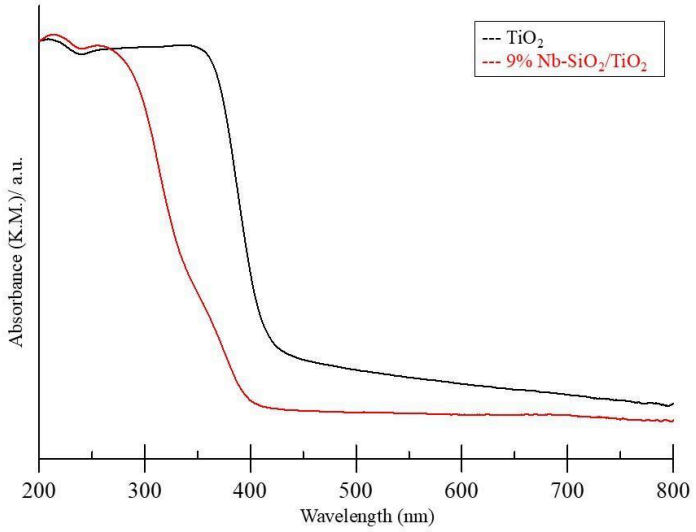

Figure 2(a) UV-Vis DRS absorption spectra of 9% Nb-SiO_2/TiO_2 and pure TiO_2

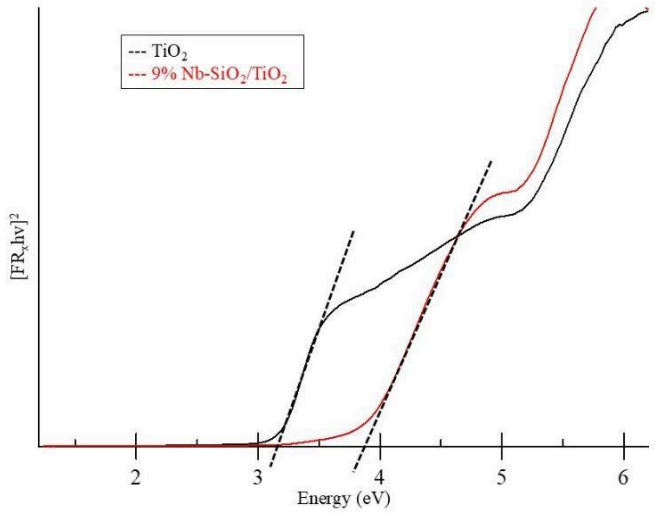

Figure 2(b) Graph of $[FR_xhv]^2$ against eV using the Tauc equation and Kubelka-Munk function

Table 1. Bandgap energy of pure TiO_2 and 9% Nb-SiO_2/TiO_2

Sample	Calculated bandgap energy, E_g (eV)
TiO_2	3.05
9% Nb-SiO_2/TiO_2	3.58

3.4 Nitrogen Adsorption-Desorption Analysis

The comparison between pure TiO_2 and the 9% Nb-SiO_2/TiO_2 composite revealed notable disparities in their textural properties, which significantly influenced their adsorption and catalytic efficacy. The Brunauer-Emmett-Teller (BET) surface area study results, illustrated in Table 2 and the nitrogen adsorption-desorption isotherm, indicated a significant disparity in the textural qualities between pure TiO_2 and 9% Nb-SiO_2/TiO_2. The surface area of 9% Nb-SiO_2/TiO_2 (322 m^2/g) was substantially higher than that of pure TiO_2 (4 m^2/g), demonstrating that the integration of Nb and SiO_2 into the TiO_2 matrix markedly suppressed particle agglomeration and grain development, leading to a considerably finer and more porous structure [20]. The increase in surface area was essential for catalytic and adsorption applications, since it offers a higher number of active sites available to reactants [20]. The total pore volume of 9% Nb-SiO_2/TiO_2 (0.17 cm^3/g) was significantly higher than that of pure TiO_2 (0.01 cm^3/g), which supported the formation of a more accessible and open porous network in the composite material [21]. The average pore width notably diminished from 13.67 nm in pure TiO_2 to 2.07 nm in the Nb-SiO_2/TiO_2 sample, signifying a transition from larger mesopores in pure TiO_2 to primarily smaller mesopores or micropores in the composite. With the pore size reduced, surface area and uniform pore structure are increased. This led to better selectivity and better interaction with smaller molecules [21].

Figure 3(a) illustrates the nitrogen adsorption-desorption isotherms of pure TiO_2 and 9% Nb-SiO_2/TiO_2. As shown in Figure 3(a), TiO_2 and 9% Nb-SiO_2/TiO_2 exhibited a type IV isotherm with a H3-type hysteresis loop, indicating the presence of mesopores with silt-like pores. In comparison with pure TiO_2, Nb–SiO_2/TiO_2 exhibits higher nitrogen uptake, indicating a larger surface area and pore volume, which prevents particle agglomeration and enhances the open porous network, thereby improving gas adsorption [22]. Figure 3(b) displays the pore size distribution curves of TiO_2 and 9% Nb-SiO_2/TiO_2. The distribution curve indicated a predominant mesoporous structure, with the majority of pores smaller than 10 nm in diameter. As compared to pure TiO_2, the Nb–SiO_2/TiO_2 composite shows a sharper and more intense peak, indicating greater pore volume and improved pore uniformity. It is possible to form well-organized mesopores by incorporating SiO_2 and Nb by inhibiting TiO_2 particle aggregation and enhancing structural stability [22].

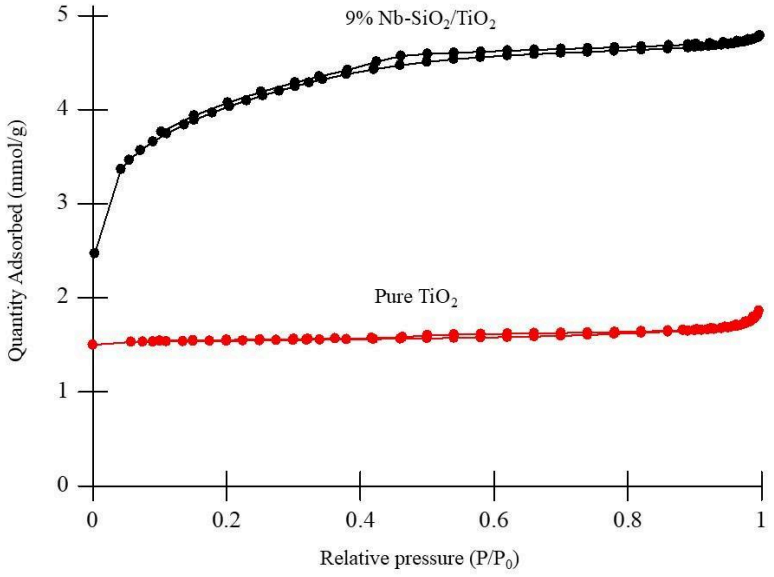

Figure 3(a) Nitrogen adsorption-desorption isotherms of pure TiO_2 and 9% Nb-SiO_2/TiO_2.

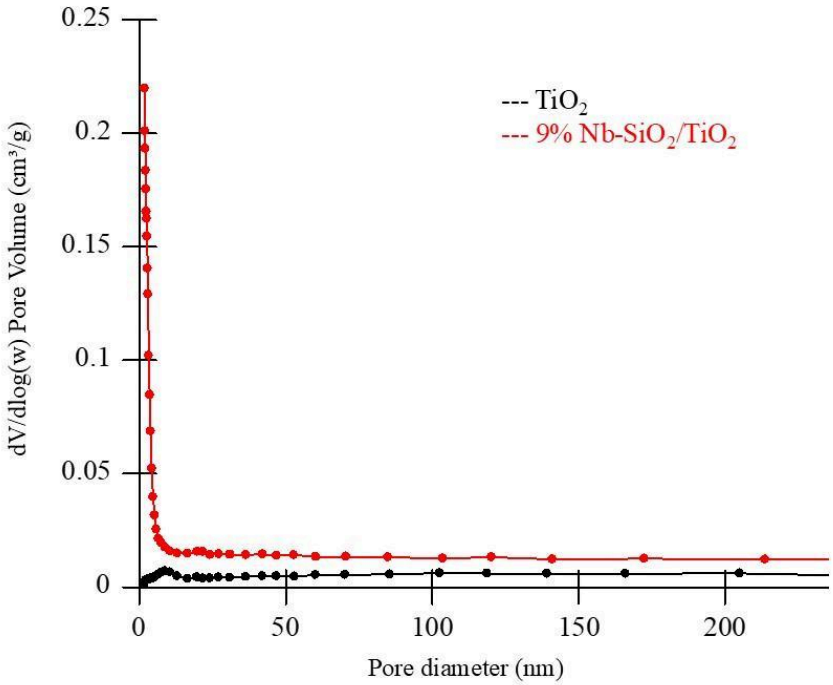

Figure 3(b) Pore distribution curves of pure TiO_2 and 9% Nb-SiO_2/TiO_2.

Table 2 Surface area, total pore volume, and average pore diameter for pure TiO_2 and 9% Nb-SiO_2/TiO_2

Sample	Surface Area (m^2/g)	Total Pore Volume (cm^3/g)	Average Pore Diameter (nm)
TiO_2	4	0.01	13.672
9% Nb-SiO_2/TiO_2	322	0.17	2.07

3.5 FTIR Spectroscopy

Figure 4 illustrates the FTIR spectra of sol-gel synthesized TiO_2 and 9% Nb-SiO_2/TiO_2 composite across the region of 400-4000 cm^{-1}. For TiO_2, the peaks at 3438.70 and 1640.26 cm^{-1} in the spectra corresponded to the stretching and bending vibrations of the -OH group. The spectrum of pure TiO_2 showed peaks at 523.88 cm^{-1}, indicating stretching vibrations of TiO_2, and peaks at 1416.38 cm^{-1}, signifying stretching vibrations of Ti-O-Ti. In contrast, for the 9% Nb-SiO_2/TiO_2 composite, the distinctive SiO_2 vibration bands were found at 466 cm^{-1} and 1100 cm^{-1}, which correlated to the bending and stretching vibrations of Si-O-Si, respectively [15]. The weak band at 2341 cm^{-1} was attributed to Nb [13]. The bands at 1651 and 3400 cm^{-1} were attributed to the stretching of O-H bonds and water hydration, respectively. At 799 cm^{-1}, a Si-O-Ti bond was detected. The absorption band at 970 cm^{-1} can be ascribed to surface Si–OH vibrations, which may also overlap with the characteristic Si–O–Ti stretching modes associated with tetrahedrally coordinated titanium species [13].

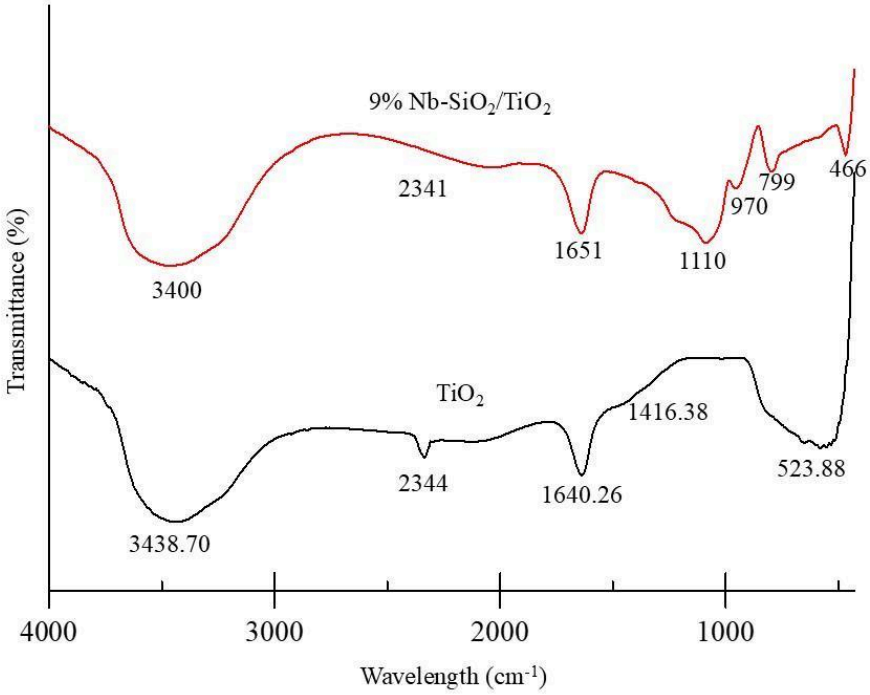

Figure 4 FTIR spectra of pure TiO_2 and 9% Nb-SiO_2/TiO_2

3.6 Photocatalytic evaluation

The contact duration between the photocatalyst and the MB solution was regularly maintained throughout the experiment, typically ranging from 60 minutes to 360 minutes, to monitor the degradation process. Samples were extracted at consistent intervals to quantify the decrease in methylene blue concentration over time. The photocatalytic removal efficiency of methylene blue of pure TiO_2 and Nb-SiO_2/TiO_2 samples is illustrated in Figure 5. Furthermore, the graph of the MB removal efficiency of MB against time with varying MB concentrations is displayed in Figure 6. In comparison to pure TiO_2, all x Nb-SiO_2/TiO_2 composites (where x = 1, 3, 5, 7, and 9 mol%) demonstrated markedly improved photocatalytic efficacy, with the removal of MB rising gradually with irradiation duration. Pure TiO_2 exhibited the lowest degradation efficiency of 16.47% after 360 minutes, underscoring its limitation in photocatalytic applications. Doping with Nb and supported SiO_2 enhanced charge carrier separation and surface properties, leading to increased degradation rates [23]. The 9% Nb-SiO_2/TiO_2 composite exhibited the highest degradation efficiency (65%), followed by 7% (63%), 5% (54%), and 3% (50%). The least-doped sample (1%) exhibited enhanced performance (32%) relative to pure TiO_2, underscoring the advantageous impact of doping on photocatalytic oxidation under visible light.

The enhanced performance was due to the synergistic interaction between niobium and silica. Niobium (Nb^{5+}) functioned as an electron trap, diminishing the recombination rates of photogenerated charge carriers, while silica enhanced surface area and more efficiently dispersed TiO_2 particles, hence improving light absorption and dye adsorption. The rising trend in MB degradation with dopant loading indicates that doping imparted advantageous structural and electrical alterations to TiO_2 [6]. The minimal performance difference between the 7% and 9% composites indicated a performance plateau, suggesting that excessively high dopant concentrations might not substantially augment activity. Nb-SiO_2/TiO_2 composites showed significant potential as effective photocatalysts for eliminating organic pollutants in wastewater treatment applications.

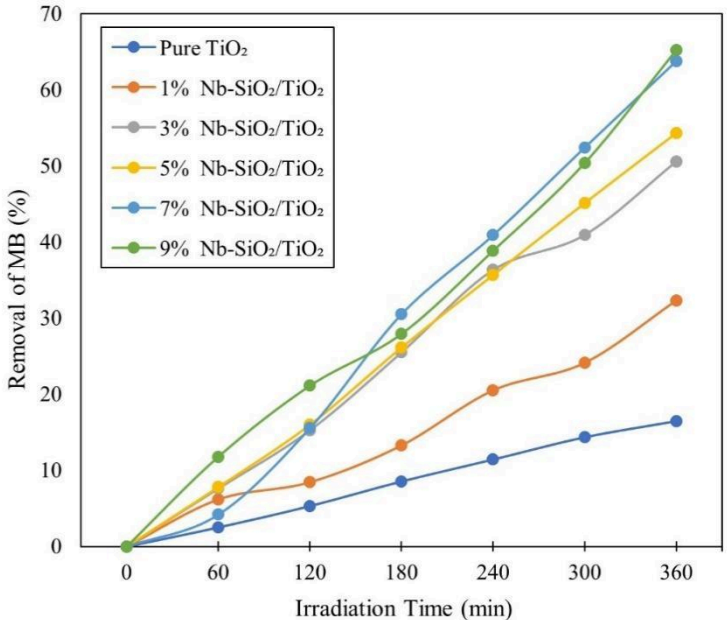

Figure 5 Removal efficiency of MB using pure TiO_2 and Nb-SiO_2/TiO_2 samples.

The 9% Nb-SiO_2/TiO_2 composite exhibited the best photocatalytic performance and was selected for further investigation under different MB concentrations. The concentrations studied were 5 ppm, 10 ppm, 15 ppm, 20 ppm, and 25 ppm to evaluate the material's degradation efficiency under varying pollutant loads. The data indicated a distinct trend in the photocatalytic degradation of MB using the Nb-SiO_2/TiO_2 composite, with degradation efficiency improving over time across all concentrations. At 5 ppm, the removal efficiency rose from 29% at 60 minutes to 84% at 360 minutes, demonstrating the catalyst's significant efficacy in degrading MB with prolonged exposure time. Similarly, for elevated concentrations of 10 ppm and 15 ppm, the removal efficiency improved over time; however, the rate of enhancement was slightly slower than that observed at lower concentrations. This was likely due to the lower MB concentrations providing increased accessible active sites on the catalyst for adsorption and degradation, facilitating a more rapid reaction.

The MB degradation rate, on the other hand, decreased with increasing concentration, indicating that the system's photocatalytic efficiency was constrained as the pollutant concentration increased. The efficacy of photocatalytic removal decreased at corresponding time intervals as the concentration of MB increased. At 360 minutes, the 5-ppm concentration achieved 84% removal efficiency, whereas at 25 ppm, the efficiency was markedly lower at 3%. This phenomenon could be explained by the saturation of the catalyst's active sites at elevated pollutant concentrations [24]. The excess MB molecules in solution overwhelmed the catalyst, reducing contact between the catalytic surface and the dye molecules. As a result, this led to reduced photodegradation efficiency. According to the results, the concentration of MB should have been carefully regulated to prevent catalyst saturation for the best photocatalytic performance [25].

360 minutes was chosen as a standardized experimental endpoint to assess photocatalytic activity across different MB concentrations, even though the system had not yet reached equilibrium. Although further degradation may occur if the reaction is prolonged beyond 360 minutes, the rate of degradation tends to diminish as the MB concentration drops. Consequently, 360 minutes offered a workable compromise between preserving experimental efficiency and identifying significant degradation trends. The percentage elimination of MB over time at various beginning concentrations is shown in Figure 5, which makes it evident how the pollutant load affects photocatalytic performance.

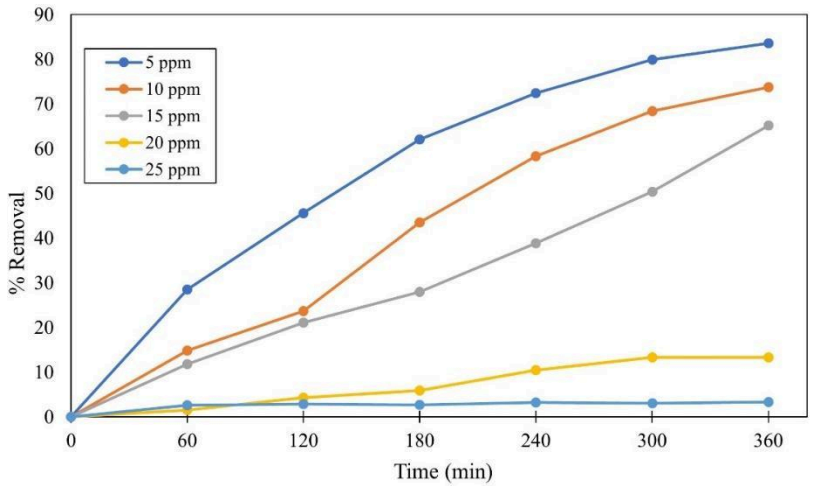

Figure 6 Removal efficiency of MB at varied concentrations using 9% Nb-SiO_2/TiO_2 sample.

4.0 CONCLUSION

A series of niobium-doped silica-titania (Nb-SiO_2/TiO_2) composites has been successfully synthesized. SiO_2/TiO_2 was synthesized using a sol-gel method, whereas 1-9% niobium-doped SiO_2/TiO_2 was synthesized through a solid-state method. XRD revealed the anatase TiO_2 phase, while the Nb-SiO_2/TiO_2 amorphous form. UV-Vis DRS indicated increased bandgap energies (3.05–3.28 eV) due to the Burstein-Moss effect, whereas FTIR confirmed the integration of Nb and Si. BET analysis revealed the larger surface area (322 m^2/g) in the 9% Nb-SiO_2/TiO_2 sample. Photocatalytic experiments with MB under visible light indicated that the 9% Nb-SiO_2/TiO_2 composite had the maximum degradation (65% at 15 ppm in 360 minutes; 84% at 5 ppm in 360 minutes). The improved performance is attributed to the increased surface area and porosity, while the synergy between the silica support and Nb doping makes the composite a sustainable material for wastewater treatment.

Acknowledgment

The authors would like to acknowledge the financial support obtained from the Ministry of Higher Education Malaysia (MOHE) and Universiti Teknologi Malaysia (UTM) through the Potential Academic Staff grant (Cost centre: QJ130000.2754.03K86). The authors are grateful to the University Industry Research Laboratory at UTM for providing research facilities, including the XRD.

References

1. Sudarshan, S., et al., *Impact of textile dyes on human health and bioremediation of textile industry effluent using microorganisms: currrent status and future prospects.* Journal of Applied Microbiology, 2022. **134**(2).
2. Nguyen, T.N.N., T.T.H. Huynh, and T.H. To, *Removal of methylene blue from simulated wastewater by Carica papaya wood biosorbent.* Vietnam Journal of Science, Technology and Engineering, 2020. **62**(4): p. 8–17.
3. Ling, C.M., S.-T. Ong, and S.L. Lee, *Recent development of surface-modified titanium dioxide for enhanced oxidation catalytic activity: A short review.* Journal of Alloys and Compounds, 2025. **1037**: p. 182226.
4. Leong, C.Y., et al., *Effect of Synthesis Methods on Properties of Copper Oxide Doped Titanium Dioxide Photocatalyst in Dye Photodegradation of Rhodamine B.* Science and Technology Indonesia, 2022. **7**(1): p. 91-97.
5. Chew, Y.B., et al., *Sonochemical Synthesis of Rutile Phase Copper-Doped Titanium Dioxide Coating on Fabric and Its Application in Antibacterial Testing of Staphylococcus aureus.* Science and Technology Indonesia, 2025. **10**: p. 605-613.
6. Ling, C.M., F.A.M. Zaid, and S.L. Lee, *Niobium Oxide Doped Titanium Dioxide Photocatalyst for Phenol Photodegradation,* Journal of Materials in Life Sciences, 2023. **2**: p. 227-233.
7. Santos, J.E.d.l.C.-d.l., et al., *Photocatalytic performance of Nd/TiO_2 and Nb/TiO_2 nanomaterials in the degradation of p-cresol at room temperature.* Journal of Chemical Technology and Biotechnology, 2024. **99**(12): p. 2509-2521.
8. Wang, H., Q. Tang, and Z. Chen, Li, T., Wang, J, *Recent advances on silica-based nanostructures in photocatalysis.* Science China Materials, 2020. **63**(11): p. 2189-2205.
9. Anucha, C.B., et al., *Titanium dioxide (TiO_2)-based photocatalyst materials activity enhancement for contaminants of emerging concern (CECs) degradation: In the light of modification strategies.* Chemical Engineering Journal Advances, 2022. **10**: p. 100262.
10. Lebeau, B., et al., *Soft-templated mesostructured TiO_2- SiO_2 composites with high thermal stability.* Microporous and Mesoporous Materials, 2024. **364**: p. 112851.
11. V.Aherkar, V., et al., *Photocatalytic dye degradation efficacy and antimicrobial potency of zinc oxide nanoparticles synthesized via sol-gel method.* Next Materials, 2025. **9**: p. 100972.
12. Sowmiya, K.C. and K.A. Vijayalakshmi, *Fabrication of $MnCo_2O_4$ electrode accustomed in energy storage devices integrating through solid-state method.* Journal of the Indian Chemical Society, 2024. **101**(9): p. 101209.
13. Lee, S.L., J.M. Ekhsan, and C.M. Ling, *Properties and Bifunctional Catalytic Activity of Niobium-Doped Silica-Titania: Effect of Phosphoric Acid Treatment.* Science and Technology Indonesia, 2022. **7**(4): p. 455-460.

14. Rosa, D., et al., *Easy way to produce iron-doped titania nanoparticles via the solid-state method and investigate their photocatalytic activity.* Journal of Materials Research, 2023. **38**: p. 1282-1292.
15. Ling, C.M., et al., *TUD-C Supported Tungsten Oxide Doped Titania Catalysts for Cyclohexane Oxidation.* Malaysian Journal of Chemistry, 2020. **22**(2): p. 29-36.
16. Adzis, N.S., et al., *Modification of Silver Oxide/Silver Doped Titanium Dioxide (Ag_2O/Ag-TiO_2) Photocatalyst Using an Immobilized Reverse Photodeposition Method for Photodegradation of Reactive Red 4 Dye.* Malaysian Journal of Chemistry, 2023. **25**(4): p. 184-198.
17. Halin, D.S.C., et al., *The Effect of Polyethylene Glycol (PEG) on TiO_2 Thin Films via Sol-Gel Method.* IOP Conference Series: Materials Science and Engineering, 2019. **743**: p. 012007.
18. Nzereogu, P.U., et al., *Silica extraction from rice husk: Comprehensive review and applications.* Hybrid Advances, 2023. **4**: p. 100111.
19. Cavallo, C., et al., *Effect of the Niobium Doping Concentration on the Charge Storage Mechanism of Mesoporous Anatase Beads as an Anode for High-Rate Li-Ion Batteries.* ACS Applied Energy Materials, 2021. **4**(1): p. 215-225.
20. Kovářík, T., et al., *Sol-gel derived silicate-phosphate glass SiO_2–P_2O_5–CaO–TiO_2: The effect of titanium isopropoxide on porosity and thermomechanical stability.* Microporous and Mesoporous Materials, 2024. **374**: p. 113138.
21. Andronic, L., C. Abreu-Jaureguí, and J. Silvestre-Albero, *Construction of TiO_2@Cu_2O-CuS heterostructures integrating RGO for enhanced full-spectrum photocatalytic degradation of organic pollutants.* Journal of Alloys and Compounds, 2024. **994**: p. 174682.
22. Nirmala, S. and M. Jose, *Enhanced electrochemical performance and photocatalytic activity of mixed-phase anatase/rutile TiO_2 @ SiO_2 core-shell nanoparticles.* Electrochimica Acta, 2025. **533**: p. 146407.
23. Wang, J., et al., *Microstructure and photocatalytic activity of TiO_2-SiO_2 composite materials.* Journal of Physics: Conference Series, 2020. **1676**: p. 012059.
24. Zyoud, A.H., *Photodegradation of aqueous tetracycline using CuS@TiO_2 composite under solar-simulated light: Complete mineralization, catalyst efficiency, and reusability.* Heliyon, 2025. **11**(2).
25. Khalk, A.A.A.E., et al., *High Degradation of Methylene Blue Using a New Nanocomposite Based on Zeolitic Imidazolate Framework-8.* ACS Omega, 2021. **6**(40): p. 26210-26220.